Constrained Model Predictive Control for Dynamic Path Tracking of a Bi-steerable Rover on Slippery Grounds

Mohamed Fnadi, Wenqian Du, Frédéric Plumet, Faïz Benamar

Constrained Model Predictive Control for Dynamic Path Tracking of a Bi-steerable Rover on Slippery Grounds

Mohamed Fnadi[1,*], Wenqian Du[1], Frédéric Plumet[1], Faïz Benamar[1]

[1]*Sorbonne University, CNRS UMR 7222*
Institut des Systèmes Intelligents et de Robotique - ISIR
F-75005 Paris - France

Abstract

The research works carried out in this paper deal with the control of a fast double-steering off-road mobile robot. Such kind of robots requires very high stable and accurate controllers because their mobility is particularly influenced by wheel-ground interactions. Hence, the vehicle dynamics should be incorporated in the control circuit to take into account these issues, which is developed based on the road geometry parameters and the slippage-friction conditions at the wheel-ground contacts. Relying on this dynamic model, we present in this paper the design and application of a constrained Model Predictive Control (MPC). It is based on the minimization of a cost function (optimizing the deviation from the reference trajectory, and the variation of the control input) along a finite prediction horizon, however, the prediction horizon is variable according to the forward speed of the robot. On the other hand, this approach incorporates several constraints, essentially important for the stability and safety of an off-road mobile robot moving at the high velocity, namely : saturation and maximum variations of the vehicle's actuators (i.e. steering joints and their speeds limits) as well as the tire adhesion zone bounds (allowing to validate the assumption of a linear tire model). The full optimization problem is formulated as a Linearly Constrained Quadratic Programming (QP) to compute at each

---

*Corresponding author
    Email address:* `mohamed.fnadi@sorbonne-universite.fr` (Mohamed Fnadi)

time-step the optimal and dynamically-consistent front and rear steering angles that are required to reach the desired path, with respect to all these constraints. The capabilities of our proposed controller are compared with another control law which does not apply any physical or intrinsic constraints. The latter is simply a feedback controller based on the same dynamic model and LQR theory (Linear Quadratic Regulator). Both of them have been investigated through several tests on simulations via ROS/GAZEBO and experiments on a real off-road vehicle for different kinds of trajectories and velocity levels.

1. Introduction

Agile autonomous off-road rovers have been used to explore and intervene effectively and securely in large areas, where it is subjected to different phenomena such as slippage and friction conditions as well as the ground roughness, both can affect the feasibility and robustness of the path or trajectory tracking tasks. Therefore, such automatic systems require extremely accurate and robust controllers enabling them to preserve their stability and safety during the executed task, in spite of the hazardous situations encountered. On the other hand, in order to move easily in cluttered environments and/or achieve paths with a small turning radius and with high flexibility, the mobile robot structure is designed such that the front and rear wheels can be steered and driven independently. This kind of four-wheel steering vehicles is demonstrated to be interesting and promising for robotics applications, essentially for the lateral dynamics control at high speeds and for the increment of the path curvature [1][2].

Even though, several approaches dedicated to indoor or on-road vehicles have already been proposed (based on the vehicle kinematics [3] or the dynamics [4]), they can not be extended to off-road vehicles which are intended to move on uneven terrain at high speed. In fact, they assume that the vehicle dynamics

2

²⁰ cannot be affected in the considered context. In other words, these kinds of controllers cannot guarantee the system stability if the contact parameters are not well-defined and when the properties between the tire/soil are expected to change [5] [6]. Authors in [7] and [8] present the main challenges and control strategies used in path following and trajectory tacking methods for autonomous

²⁵ ground vehicles.

To improve their safety and manoeuvrability, mainly at high speeds, many strategies have been explored in robotics literature. At the hardware level, the mechanical design can be optimized to reduce the apparent inertia of the robot and make it lightweight [9]. In addition, compliant components can be added to

³⁰ enable smoother inclinations of the vehicle and less severe impacts (e.g. during cornering). For instance in [10] and [11], an active anti-roll system was designed and mounted on the vehicle's chassis with independent suspensions to minimize the lateral load transfer (LLT) during cornering, and minimize the consumed energy by the actuators. However, the stability control via this kind of the

³⁵ active anti-roll barre is sometimes very complex and is not easy to manage, thus the system performance can then be degraded.

At the control level, safe navigation on natural environment requires : i) switching between different control modes (acceleration and braking) without causing potentially harmful discontinuities in the movements of the robot ; ii)

⁴⁰ the formulation of safety and stability indicators to reflect the amount of authorized admissible bounds on the dynamic behavior of the robot, to be easily accounted for, the possibility to express these safety criteria as constraints related to the control inputs of the robot. By the way, this is done by introducing the appropriate constraints characterizing the stability and safety conditions in

⁴⁵ the trajectory planning and control. Authors in [12] present a 4-wheel steering controller to track a reference yaw rate and the side-slip signals while incorporating an anti-windup technique to reduce the effects of the saturation of the rear steering actuators. [13] considers a stability domain such that the harsh curvatures and the wide variation in the robot's forward speed are prevented.

⁵⁰ Moreover, authors in [14] and [15] present a control scheme for automatic path

3

tracking which subjects to wheel sleep constraint. In addition, [16] presents an online path generator for a wheeled robot taking into account the contact constraints and joints' velocity and acceleration limits.

On the other hand, Model Predictive Control (MPC) technique has been widely used in the automotive and industrial process because of its ability to simply handle system nonlinearities and constraints on inputs and states as well as its capability to anticipate future changes in set-points, i.e. the future reference trajectory. It has been shown to be much more interesting and sophisticated for solving linear or nonlinear path planning and control problems [17]. Besides that, Nonlinear MPC (NMPC) is usually solved using a sequential quadratic programming method (SQP) [18] and/or the DynIbex library which is based on Runge-Kutta schemes to solve the initial value problem of ordinary differential equations and of differential-algebraic equations [19]. As an example, authors in [20] introduced a NMPC controller implemented on a single steering vehicle for path following, where the problem is solved at each sampling instant using SQP. Moreover, papers [21] and [22] make use of a spatial NMPC for path planning and control problems, which are divided into the upper and lower levels applying constraints on the vehicle's position in the lane. Furthermore, [23] and [24] introduce a reliable and guaranteed NMPC approach based on interval analysis including the model uncertainties, where the problem is solved at each sampling instant using the DynIbex library. Nevertheless, it has been shown that the fast convergence of this kind of solvers is not guaranteed over a finite time (i.e. huge response time to get the solution of the problem), because of its computational complexity. Therefore, they are generally limited to low vehicle speeds and/or indoor applications (such as in the logistics and industry field). To overcome this issue and still decrease the computational complexity, the linear MPC seems much more attractive for various classes of fast applications, such as in the mining and agriculture fields, because in general the optimization problem is completely specified as a Quadratic Program (QP), which can be easily handled by linear solvers. For example, in [25] and [26], a Linear Time Varying MPC technique is presented to tackle the same problem. It is based

4

on the on-line exact linearization of the nonlinear vehicle model and the linear MPC technique to control the front steering angle and stabilize the vehicle on slippery roads (snow-covered) at higher speeds.

₈₅ In order to properly account for the safety and stability constraints related to the sliding and steering parameters, the control problem is expressed as a Linearly Constrained Quadratic Program (QP). The adequate front and rear steering angles are calculated to perform a trajectory tracking in the operational space is subject to several linear inequality constraints accounting for ₉₀ the physical limitations of the robot (steering joint limits and their variation bounds) as well as for the limit values on the sliding parameters (i.e. tire adhesion area bounds to maintain the linear tire model hypothesis). To demonstrate its efficiency, the proposed control framework is expected to be compared with another controller described in [27]. This latter method is based on the LQR ap- ₉₅ proach and the same dynamic model used for the constrained MPC. Although, no necessary constraint is taken into account by this LQR controller to compute adequate steering angles, it is a beneficial point to emphasize the importance of the constraints and the predictive strategy. Moreover, this paper presents, simulation results from the high fidelity virtual platform using ROS/GAZEBO, ₁₀₀ as well as, results from the field tests demonstrating the effectiveness of our proposed approach compared with the LQR controller via the experimental platform, "*SPIDO*" robot, along different paths and different speeds.

This paper is structured as follows, in section 2, the linear tire model and the wheeled dynamic modeling for double-steering vehicles are presented. In ₁₀₅ Section 3, the controller is derived: tasks-related objectives are formulated and the inequality safety related constraints acting on the system are expressed as a function of the control inputs of the system, i.e. front and rear steering angles. In Section 4, the results of the simulations and the experiments are introduced and discussed, on which the capabilities offered by the proposed controller are ₁₁₀ illustrated and compared with those provided by the LQR controller. Finally, Section 5 summarizes the contribution and provides an overview of the future work.

2. Wheeled Mobile Robot Modeling

2.1. Linear Tire Model

115   The notations for the vehicle dynamics and the path tracking task are introduced in Table 1.

Since the sliding parameters and tire-ground forces have been incorporated into the lateral vehicle dynamics, a contact model must be chosen to describe the longitudinal and lateral tire forces. In the literature, several kinds of models

120   can be used to describe the slippage phenomenon (e.g., Pacejka model [28], Dugoff model [29] and Fiala tire model [30]). For on-road or off-road vehicles, three zones can be distinguished even if these tire models are physically and analytically different (cf. Figure 1), and they can be presented as,

① At low slippage, the lateral force $F_{y(f,r)}$ generated by the tire is almost

125   linear with the slip angle $\beta_{(f,r)}$ (i.e. angle between the wheel's velocity vector and its longitudinal axis). The proportionality coefficient refers to the lateral tire cornering stiffness $C_{(f,r)}$, which is particularly depending on the grip conditions variations, the loaded normal forces and the friction coefficient.

130 ② Since the slip angle increases, the transition area is achieved. The lateral force at the tire contact reaches the friction limit related to the normal force and the friction coefficient (μF_z).

③ When the slip angle exceeds a certain value due to the slippery conditions and the centrifugal force (e.g., during cornering), the tire-ground

135   forces are extremely non-linear, in which the robot drifts and becomes uncontrollable.

To simplify the tire forces model, our robot is assumed to always run in the pseudo-sliding area (zone ①) Therefore, the lateral force is proportional to the slip angle with the cornering stiffness. This relationship can simply be expressed
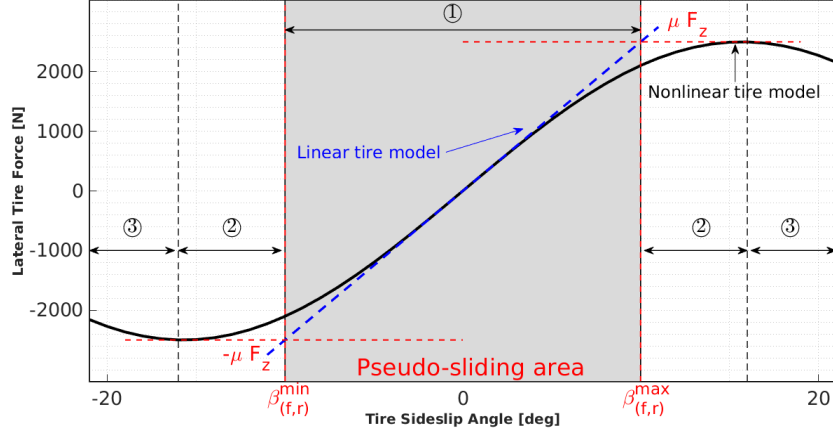
6

Figure 1: Illustration of a generic nonlinear tire curve for lateral slippage with different zones, reduced to a pseudo-sliding area where the wheels offer the best grip conditions.

as follows,

$$F_{yf} = C_f \beta_f, \tag{1a}$$

$$F_{yr} = C_r \beta_r, \tag{1b}$$

2.2. Vehicle dynamics modeling

Relying on the bicycle model representation shown in Figures 2 and 3, the linear tire model given by the equation (1) and assuming that the longitudinal velocity V_x is constant and the longitudinal forces F_{xi} is neglected, the lateral vehicle dynamics can be derived as the linear state-space representation by applying the Newton's law at the center of gravity (CoG) of the vehicle,

$$\begin{cases} \dot{\xi} = A(\xi - \xi_{ss}) + B(u - u_{ss}) \\ y = C(\xi - \xi_{ss}) \end{cases} \tag{2}$$

where $\xi = [V_y, V_\psi, e_y, e_\psi]^T$ is the state vector, $u = [\delta_f, \delta_r]^T$ denotes the input vector (steering angles) and $y = [V_\psi, e_y, e_\psi]^T$ represents the output vector (V_ψ,

7

Table 1: Notations for the lateral vehicle dynamics and path tracking task.

Symbol	Meaning
Γ_r	reference path to be followed
$\mathcal{R}_\mathrm{i} = \{O, X, Y, Z\}$	absolute global frame(or inertial frame)
p_G	center of mass of the vehicle
p_F	closest point on the path
$\mathcal{R}_\mathrm{G} = \{x_\mathrm{G}, y_\mathrm{G}, z_\mathrm{G}\}$	frame attached to the vehicle body
$\mathcal{R}_\mathrm{wi} = \{x_\mathrm{wi}, y_\mathrm{wi}, z_\mathrm{wi}\}$	frame attached to the wheel i
$\mathcal{R}_\mathrm{F} = \{x_\mathrm{F}, y_\mathrm{F}, z_\mathrm{F}\}$	Serret-Frenet that moves along the path
e_y	lateral error between p_G and p_F
e_ψ	angular error
ρ	curve curvature
θ_r	road slope angle
ϕ_r	road bank angle
ϕ_s	suspension deflection angle
δ_f, δ_r	front and rear steering angles, respectively
β_f, β_r	front and rear side-slip angles, respectively
C_f, C_r	front and rear tire cornering stiffnesses, respectively
F_{xi}	longitudinal force at the wheel $i \in \{f, r\}$, expressed in $\mathcal{R}_\mathrm{G}$
F_{yi}	lateral force at the wheel $i \in \{f, r\}$, expressed in $\mathcal{R}_\mathrm{G}$
F_{zi}	vertical force at the wheel $i \in \{f, r\}$, expressed in $\mathcal{R}_\mathrm{G}$
a, d	front and rear half-wheelbases and track width
ψ, ψ_d	vehicle and reference yaw angles, respectively
V_x, V_y, V_ψ	longitudinal and lateral velocities and yaw rate, respectively
μ	tire/road friction coefficient
m, I_z	vehicle mass and yaw-inertia moment, respectively
g	acceleration due to gravity
a_y	lateral acceleration

e_y and e_ψ are measured with the embedded sensors and V_y is observed by a Kalman-Bucy filter reminded in Appendix B). ξ_{ss} and u_{ss} describe the steady-state vectors of the linear model with drift, which depend mainly on the gravity parameters (sloping grounds).

$$
A = \begin{bmatrix} a_{11} & a_{12} & 0 & 0 \\ a_{21} & a_{22} & 0 & 0 \\ 1 & 0 & 0 & V_x \\ 0 & 1 & \rho^2 V_x & 0 \end{bmatrix} = \begin{bmatrix} -2\dfrac{C_f + C_r}{mV_x} & -2\dfrac{aC_f - aC_r}{mV_x} - V_x & 0 & 0 \\ -2\dfrac{aC_f - aC_r}{I_z V_x} & -2\dfrac{a^2 C_f + a^2 C_r}{I_z V_x} & 0 & 0 \\ 1 & 0 & 0 & V_x \\ 0 & 1 & \rho^2 V_x & 0 \end{bmatrix},
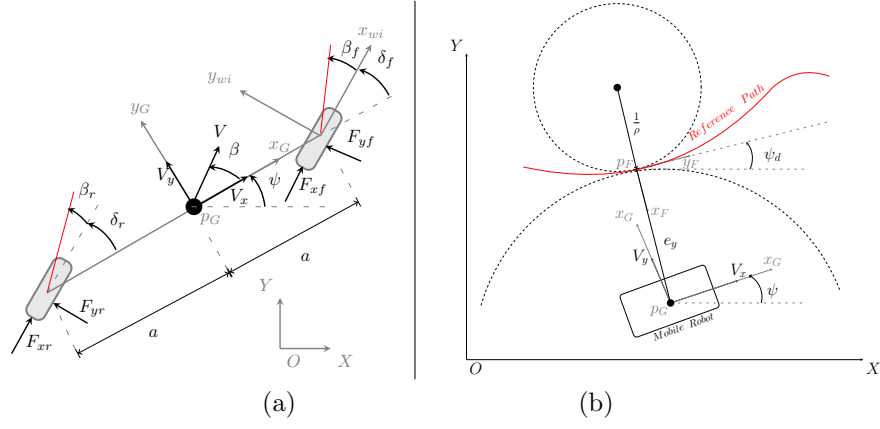$$

8

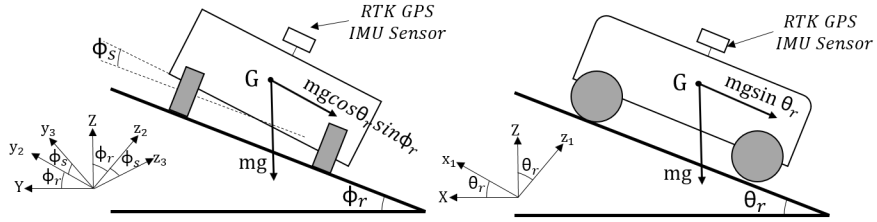Figure 2: (a) Dynamic bicycle model with sliding parameters in yaw frame. (b) Path following notation.

Figure 3:   Road grade angle [Left] and bank angle [Right].

$$B = \begin{bmatrix} b_{11} & b_{12} \\ b_{21} & b_{22} \\ 0 & 0 \\ 0 & 0 \end{bmatrix} = \begin{bmatrix} \dfrac{2C_f}{m} & \dfrac{-2C_r}{m} \\ \dfrac{2aC_f}{I_z} & \dfrac{2aC_r}{I_z} \\ 0 & 0 \\ 0 & 0 \end{bmatrix} \quad C = \begin{bmatrix} 0 & 1 & 0 & 0 \\ 0 & 0 & 1 & 0 \\ 0 & 0 & 0 & 1 \end{bmatrix},$$

$$u_{ss} = \begin{bmatrix} \dfrac{\rho V_x(a_{11}a_{22} - a_{21}a_{12}) - a_{21}g\cos\phi_r\sin\theta_r}{a_{21}(b_{11} - b_{12}) - a_{11}(b_{21} - b_{22})} \\[2em] \dfrac{-\rho V_x(a_{11}a_{22} - a_{21}a_{12}) + a_{21}g\cos\phi_r\sin\theta_r}{a_{21}(b_{11} - b_{12}) - a_{11}(b_{21} - b_{22})} \end{bmatrix},$$

9

$$\xi_{ss} = \begin{bmatrix} \dfrac{\rho V_x[a_{22}(b_{11} - b_{12}) - a_{12}(b_{21} - b_{22})] - g\cos\phi_r\sin\theta_r(b_{21} - b_{22})}{a_{11}(b_{21} - b_{22}) - a_{21}(b_{11} - b_{12})} \\ \rho V_x \\ 0 \\ \dfrac{-\rho V_x[a_{22}(b_{11} - b_{12}) - a_{12}(b_{21} - b_{22})] + g\cos\phi_r\sin\theta_r(b_{21} - b_{22})}{V_x(a_{11}(b_{21} - b_{22}) - a_{21}(b_{11} - b_{12}))} \end{bmatrix}$$

The continuous-time state space model (2) can be discretized following the zero-order-hold method (ZOH). It is therefore relatively easy to calculate an approximate discrete-time model for a small sampling time denoted T_d by using the forward differences,

$$\begin{cases} X_{k+1} = \Phi X_k + \Gamma U_k, \\ y_k = C X_k, \end{cases} \tag{3}$$

where $\Phi = I_{4\times4} + T_d A$ and $\Gamma = T_d B$ are respectively the state and command matrices of the discrete-time state-space model, I denotes the identity matrix, $X_k = \xi_k - \xi_{ss}$ and $U_k = u_k - u_{ss}$ are respectively the state and input vectors.

3. Constrained Model Predictive Controller

In this section a dynamic control strategy based on a constrained model predictive controller (MPC) that ensures the safety and stability of the off-road mobile robot. The main purpose is to compute the optimal steering angles required to perform a trajectory tracking task while respecting a number of constraints at each sampling instant. These constraints are summarized as below :

- Conform with the tire pseudo-sliding area by maintaining the slip angles between two given values (cf. Figure 1).

- Respect the limits of steering actuators (i.e., the front and rear steering angles must be limited according to the articulated stops);

- Avoid large steering variations to ensure the vehicle stability and safety. In order to do this, the steering velocity must also be saturated.

10

3.1. Path tracking task formulation

The main contribution of this paper lies on the application of the proposed constrained MPC to the fast off-road rover. This controller is based on the minimization of a quadratic objective function that is composed by the error between the desired path and the predicted output. The main advantage of the MPC is indeed the ability to anticipate future changes in setpoints and handle constraints that are critical and necessary for the safety and stability of the vehicle. Otherwise, MPC is based on the principal of the output y prediction at each time-step k over a finite time interval $[kT_d, (k + N_p)T_d]$, where the prediction horizon N_p is usually tuned according to the forward vehicle velocity. At the next time-step, $k + 1$, a new optimal control problem based on new measurements of the updated state is solved over the shifted horizon (see [31] for an overview of the basics of MPC theory).

To introduce the design of the constrained MPC, the vehicle dynamic model (3) can be derived in the recursive augmented form, by iterating this model N_p times in order to relate the predicted output $y_{k+i|k}$ and input $U_{k+i|k}$ at step time $k + i$, which are both computed from the instant k. The dynamic model can be simply written in the augmented presentation as follows :

$$Y = P_x X_k + P_u U, \tag{4}$$

$$\text{where} \quad Y = \begin{bmatrix} y_{k+1|k} \\ y_{k+2|k} \\ \vdots \\ y_{k+N_p|k} \end{bmatrix}, \quad P_x = \begin{bmatrix} C\Phi \\ C\Phi^2 \\ \vdots \\ C\Phi^{N_p} \end{bmatrix}, \quad U = \begin{bmatrix} U_k \\ U_{k+1} \\ \vdots \\ U_{k+N_p-1} \end{bmatrix},$$

$$P_u = \begin{bmatrix} C\Gamma & 0 & \dots & 0 \\ C\Phi\Gamma & C\Gamma & \dots & 0 \\ \vdots & & \ddots & \vdots \\ C\Phi^{N_p-1}\Gamma & \dots & C\Phi\Gamma & C\Gamma \end{bmatrix},$$

11

The proposed controller computes at each sampling time the optimal steering angles U defined as a sequence of control inputs over the prediction horizon N_p by minimizing the norm of the inputs and the error between the predicted outputs Y and the reference Y_d. From (4), the cost function can be expressed in the following quadratic form :

$$J(U) = \|Y - Y_d\|_{Q_n}^2 + \|U\|_{R_n}^2, \tag{5a}$$

$$= \|P_x X_k + P_u U - Y_d\|_{Q_n}^2 + \|U\|_{R_n}^2, \tag{5b}$$

where $\|a\|_Q$ denotes the $Q-$weighted euclidean norm of a. To simplify the notation, we denote $q = 3 \times N_p$ and $r = 2 \times N_p$ (i.e, the dynamic model (3) is a multi-input multi-output system (MIMO) with 2 inputs and 3 outputs). Therefore, $Q_n \in \mathbb{R}^{q \times q}$ and $R_n \in \mathbb{R}^{r \times r}$ are both positive semi-definite weighting matrices. Y_d is the reference vector projected along the horizon prediction N_p that can be written as follows:

$$Y_d = \begin{bmatrix} y_{d\ k+1|k} \\ y_{d\ k+2|k} \\ \vdots \\ y_{d\ k+N_p|k} \end{bmatrix}, \tag{6}$$

The objective function (5b) then takes the form,

$$J(U) = \frac{1}{2} U^T H U + f^T U + E^T Q_n E, \tag{7a}$$

$$H = 2(P_u^T Q_n P_u + R_n),$$

$$E = P_x X_k - Y_d,$$

$$f = 2P_u^T Q_n E,$$

where U is the optimization vector. H is the Hessian matrix, and which has to be positive-definite in order to ensure the existence of a unique optimal solution U minimizing $J(U)$. The vector f describes the linear part of the quadratic

12

function, whereas the term $E^T Q_n E$ is not related to the optimization vector U and does not affect its computation.

3.2. Constraints formulation

3.2.1. Pseudo-sliding area bounds and tire adhesion

The MPC controller is based on a linear tire model assuming that the lateral force $F_{y(f,r)}$ varies linearly with the slip angle $\beta_{(f,r)}$ (see Figure 1). This assumption characterizes the pseudo-sliding zone where the grip conditions are the best at the tire-ground contact. Nevertheless, when the contact force exceeds some certain values, the skidding zone is reached, and the vehicle becomes uncontrollable over short time horizon. Moreover, the bad grip conditions can generate perturbations influencing the accuracy of tracking task and vehicle drifts, especially at high speeds and during sudden turn. To prevent this case, a constraint describing pseudo-sliding area bounds must be accounted. These constraints for the front and rear slippage angles $\beta_{(f,r)}$ can be derived as following (cf. Figure 1),

$$\beta_f^{min} \leq \beta_{f,k} \leq \beta_f^{max}, \tag{8a}$$

$$\beta_r^{min} \leq \beta_{r,k} \leq \beta_r^{max}, \tag{8b}$$

where $\beta_{(f,r)}^{min}$ and $\beta_{f,r}^{max}$ are the limits of the tire adhesion area computed taking into account the friction limit (μF_z). We define the side-slip angle $\beta_{f,r}$ as the angle between the wheel velocity v_{wi} and its longitudinal axis x_{wi}. These angles can be derived as a linear function with steering angles $\delta_{(f,r)}$ and vehicle velocities V_y, V_x and V_ψ. These relationships are expressed thus:

$$\beta_{f,k} = \frac{V_{y,k} + aV_{\psi,k}}{V_x} - \delta_{f,k}, \tag{9a}$$

$$\beta_{r,k} = \frac{V_{y,k} - aV_{\psi,k}}{V_x} - \delta_{r,k}, \tag{9b}$$

As it has been highlighted, this paper focuses on controlling the vehicle lateral motion at high velocities (path tracking) while fulfilling its physical and

13

intrinsic constraints. The equation (9) can be written in a matrix format depending on the state and inputs vectors,

$$\beta_k = \begin{bmatrix} \beta_{f,k} \\ \beta_{r,k} \end{bmatrix}, \tag{10a}$$

$$= T\xi_k + Ju_k, \tag{10b}$$

$$= T(X_k + \xi_{ss}) + J(U_k + u_{ss}), \tag{10c}$$

with $\quad T = \begin{bmatrix} \dfrac{1}{V_x} & \dfrac{a}{V_x} & 0 & 0 \\ \dfrac{1}{V_x} & \dfrac{-a}{V_x} & 0 & 0 \end{bmatrix} \quad$ and $\quad J = \begin{bmatrix} -1 & 0 \\ 0 & -1 \end{bmatrix},$

From (10c), the side-slip angles over a moving time horizon N_p can be projected as follows,

$$\underbrace{\begin{bmatrix} \beta_{k+1} \\ \beta_{k+2} \\ \vdots \\ \beta_{k+N_p} \end{bmatrix}}_{\bar{\beta} \in \mathbb{R}^{r \times 1}} = \underbrace{\begin{bmatrix} TX_{k+1} \\ TX_{k+2} \\ \vdots \\ TX_{k+N_p} \end{bmatrix}}_{\Xi} + \underbrace{\begin{bmatrix} JU_{k+1} \\ JU_{k+2} \\ \vdots \\ JU_{k+N_p} \end{bmatrix}}_{\Theta} + \underbrace{\begin{bmatrix} T\xi_{ss} + Ju_{ss} \\ T\xi_{ss} + Ju_{ss} \\ \vdots \\ T\xi_{ss} + Ju_{ss} \end{bmatrix}}_{\Pi}, \tag{11}$$

Relying on the vehicle dynamics (3), the matrix Ξ given in (11) can be developed as a function of the optimization variable U,

$$\Xi = WX_k + ZU, \tag{12}$$

$$W = \begin{bmatrix} T\Phi \\ T\Phi^2 \\ \vdots \\ T\Phi^{N_p} \end{bmatrix}, \qquad Z = \begin{bmatrix} T\Gamma & 0 & \dots & 0 \\ T\Phi\Gamma & T\Gamma & \dots & 0 \\ \vdots & \ddots & \ddots & \vdots \\ T\Phi^{N_p-1}\Gamma & \dots & T\Phi\Gamma & T\Gamma \end{bmatrix},$$

Similarly, Θ can be written as,

$$\Theta = \Upsilon U, \tag{13}$$

14

$$\text{with} \quad \Upsilon = \begin{bmatrix} 0 & J & \dots & 0 & 0 \\ 0 & 0 & J & \dots & 0 \\ \vdots & \vdots & & \ddots & J \\ 0 & 0 & \cdots & & J \end{bmatrix},$$

From (11), (12) and (13) we can finally express the projected side-slip angles $\bar{\beta}$ as following,

$$\bar{\beta} = (Z + \Upsilon)U + WX_k + \Pi, \tag{14}$$

where $W \in \mathbb{R}^{r \times 4}$, $Z \in \mathbb{R}^{r \times r}$, $\Upsilon \in \mathbb{R}^{r \times r}$ and $\Pi \in \mathbb{R}^{r \times 1}$.

Therefore, the slippage-angle constraints can be deduced using (14),

$$\begin{bmatrix} Z + \Upsilon \\ -Z - \Upsilon \end{bmatrix} U \leq \begin{bmatrix} \bar{\beta}^{\max} - WX_k - \Pi \\ -\bar{\beta}^{\min} + WX_k + \Pi \end{bmatrix}, \tag{15}$$

where $\bar{\beta}^{\max} = -\bar{\beta}^{\min} = [\beta_f^{\max}, \beta_r^{\max}, \dots, \beta_f^{\max}, \beta_r^{\max}]^T \in \mathbb{R}^{r \times 1}$ are the minimum and maximum bounds of the pseudo-sliding zone.

After the development of the slippage constraint (15), the following question must be addressed: how can we proceed to determine the limits $\bar{\beta}^{\max}$ and $\bar{\beta}^{\min}$? In fact, these saturations are related to the tire/ground contact friction coefficient μ and the normal force of the vehicle (F_z). Thus, the following inequality can be deduced using the linear tire model (1) by supposing the symmetry of the vehicle,

$$-\mu F_z \quad \leq \quad C_{(f,r)}\beta_{(f,r)} \quad \leq \quad \mu F_z \tag{16}$$

The vertical force F_z can be calculated assuming that the total weight of the vehicle is equally balanced between the front and rear axles ($F_z = \frac{mg}{2}$). Hence, the front and rear side-slip angle bounds can be approximated as,

$$\beta_f^{\min} = -\frac{\mu mg}{2.C_{(f,r)}} \quad \leq \quad \beta_{(f,r)} \quad \leq \quad \beta_f^{\max} = \frac{\mu mg}{2.C_{(f,r)}} \tag{17}$$

3.2.2. Steering angles bounds

From a practical point of view, the limitations corresponding to the articular physical capabilities of the robot must be accounted for solving the control problem. Therefore, the front and rear steering angles $\delta_{(f,r)}$ must be saturated, which is ultimately due to the fact that the vehicle's actuators have mechanical limit strokes that cannot be exceeded. These constraints can thus be expressed as following:

$$-\delta_f^{\max} \leq \delta_{f,k} \leq \delta_f^{\max}, \tag{18a}$$

$$-\delta_r^{\max} \leq \delta_{r,k} \leq \delta_r^{\max}, \tag{18b}$$

We can then derive these constraints over the prediction horizon N_p as a function of the optimization variable U, given by the the following inequality,

$$\begin{bmatrix} I_{r \times r} \\ -I_{r \times r} \end{bmatrix} U \leq \begin{bmatrix} U^{\max} - \Lambda_{ss} \\ -U^{\min} + \Lambda_{ss} \end{bmatrix}, \tag{19}$$

where $U^{\max} = -U^{\min} = [\delta_f^{\max}, \delta_r^{\max}, \ldots, \delta_f^{\max}, \delta_r^{\max}]^T \in \mathbb{R}^{r \times 1}$ are the robot's joints limits, and $\Lambda_{ss} = [u_{ss}, u_{ss}, \ldots, u_{ss}]^T \in \mathbb{R}^{r \times 1}$ denotes the vector depending on the steady-state conditions.

3.2.3. Rate of change in steering angles limits

In an equivalent way, the steering actuators have a certain maximum speed that the controller must respect at each computation step. In other words, the high variation in steering angles with the actuators' response time issue may indeed generate delays in input computation, as well as perturbations of the path tracking task. Consequently, the rate of change of the steering angles ΔU must also lie within a specific allowable range to respect the technical capabilities of the actuators. Taking these constraints into account, the quadratic programming generates smooth inputs without any abrupt changes enabling the lateral stability of the vehicle to be maintained (particularly at high speeds and during cornering). Therefore, the variation of U over the prediction horizon N_p can

simply be deduced as follows,

$$
\underbrace{\begin{bmatrix} \Delta U_k \\ \Delta U_{k+1} \\ \vdots \\ \Delta U_{k+N_p-1} \end{bmatrix}}_{\Delta U} = \underbrace{\begin{bmatrix} U_k \\ U_{k+1} \\ \vdots \\ U_{k+N_p-1} \end{bmatrix}}_{U} - \underbrace{\begin{bmatrix} U_{k-1} \\ U_k \\ \vdots \\ U_{k+N_p-2} \end{bmatrix}}_{\Omega} , \tag{20}
$$

The vector Ω can then be written as :

$$
\Omega = \underbrace{\begin{bmatrix} U_{k-1} \\ 0 \\ \vdots \\ 0 \end{bmatrix}}_{M} + \underbrace{\begin{bmatrix} 0 & 0 & \cdots & 0 \\ I_{2\times2} & 0 & \cdots & 0 \\ \vdots & \ddots & & \vdots \\ 0 & \cdots & I_{2\times2} & 0 \end{bmatrix}}_{F} \underbrace{\begin{bmatrix} U_k \\ U_{k+1} \\ \vdots \\ U_{k+N_p-1} \end{bmatrix}}_{U} , \tag{21}
$$

The variation of steering angles can then be expressed by substituting (21) into (20),

$$
\underbrace{\begin{bmatrix} \Delta U_k \\ \Delta U_{k+1} \\ \vdots \\ \Delta U_{k+N_p-1} \end{bmatrix}}_{\Delta U} = \underbrace{\begin{bmatrix} U_k \\ U_{k+1} \\ \vdots \\ U_{k+N_p-1} \end{bmatrix}}_{U} - \underbrace{\begin{bmatrix} U_{k-1} \\ 0 \\ \vdots \\ 0 \end{bmatrix}}_{M} - \underbrace{\begin{bmatrix} 0 & 0 & \cdots & 0 \\ I_{2\times2} & 0 & \cdots & 0 \\ \vdots & \ddots & & \vdots \\ 0 & \cdots & I_{2\times2} & 0 \end{bmatrix}}_{F} \underbrace{\begin{bmatrix} U_k \\ U_{k+1} \\ \vdots \\ U_{k+N_p-1} \end{bmatrix}}_{U} ,
$$
$$ \tag{22} $$

Therefore, the rate of change in steering angles as a function of optimization variable U appears to be simply,

$$
\Delta U = (I_{r\times r} - F)U - M, \tag{23}
$$

with $F \in \mathbb{R}^{r\times r}$ and $M \in \mathbb{R}^{r\times 1}$.

By exploiting (23), the constraints related to the rate of change of the front

17

and rear steering angles can naturally be written as inequality,

$$
\begin{bmatrix} I_{r \times r} - F \\ -I_{r \times r} + F \end{bmatrix} U \leq \begin{bmatrix} \Delta U^{\max} + M \\ -\Delta U^{\min} - M \end{bmatrix},
\tag{24}
$$

where $\Delta U^{\max}$ and $\Delta U^{\min}$ are the maximal and minimal permitted speeds of the steering actuators defined along N_p.

₂₄₀ 3.3. Final quadratic problem

By way of reminder, the constrained MPC strategy should be able to provide a unique optimal control input $U^\star = [U_k^\star, U_{k+1}^\star, \ldots, U_{k+N_p-1}^\star]^T$ at each time-step k that minimizes the cost function describing the trajectory tracking task, and that must be such that the considered limits are not violated at the next time step $k + 1$. The final MPC optimization problem will be recast into the standard quadratic programming (QP) formulation as following :

$$
\begin{cases} U^\star = \underset{U}{\arg\min} \quad \dfrac{1}{2} U^T H U + f^T U + E^T Q_n E, \\ \text{s.t.} \qquad G U \leq h, \end{cases}
\tag{25}
$$

where G and h gather all the linear constraints with their bounds given in (15), (19) and (24). It can be shown that the quadratic forms composing the tasks expression can be written as a function of positive semi-definite matrices including constraints expressed in a linear form (i.e. the Hessian matrix H is a function of $Q_n \in \mathbb{R}^{q \times q}$ and $R_n \in \mathbb{R}^{r \times r}$ that are chosen with positive semi-definite matrices, then H may be symmetric positive semi-definite). This QP optimization problem is then convex and admits a unique global minimum.

Since the tire/ground contact conditions are intended to be changed in the off-road context, their estimation is necessary to enhance the robustness of the QP (25). This estimation is not the subject of this paper. However, our controller is mixed with some previous works [32] and [6], summarized in the Appendix A. These algorithms are based on the dynamic model for cornering stiffnesses $C_{(f,r)}$ as well as the bank and grade angles (θ_r and ϕ_r) estimation.

4. Simulation and Experimental Validation

Simulation and experiments are conducted to evaluate the capability of the proposed controller. In order to do this, we compare the performance of our controller with another path tracking controller proposed in [27]. The second path tracking controller is based on LQR approach and the vehicle dynamic model given in (2). A brief summary of this LQR controller is presented in Appendix C. The advantage of this comparison relates to the fact that this LQR controller does not take into account any physical or intrinsic constraints.

The constrained MPC and LQR controllers are both tested on a bi-steerable mobile robot "*SPIDO*" shown in Figure 4 with a weight of $880kg$, a yaw-inertia moment of $300kg.m^2$ and a front and rear half-wheelbases of $0.85m$. The global QP problem is implemented using the CVXOPT solver, a real-time and effective open-source solver for convex optimization based on the Python programming language [33].
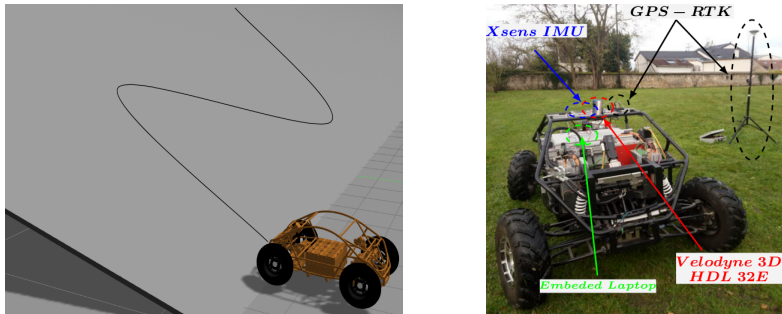

Figure 4: [Left] Virtual "*SPIDO*" platform on sloping environment. [Right] Experimental robot with the embedded sensors [34].

Our algorithms make use of two embedded sensors : First, a Real Time Kinematic GPS (RTK-GPS) providing an accurate absolute position according to the base station. This kind of GPS enables us to reach the $cm-$level accuracy at sampling frequency of $10Hz$. Second, an IMU (Xsens MTi-G) that integrates multi-axes, accelerometers, gyroscopes, and other sensors to provide an estimation of the vehicle attitude in inertial frame (e.g. yaw angle and its rate) by using EKF filter ($0.1.s^1$ accuracy at $100Hz$ sampling rate). Other sensors depicted in Figure 4 (e.g. LiDAR) are not exploited in the framework of

19

this paper. Otherwise, the lateral velocity V_y used by our approach needs to be observed. That is why a linear Kalman-Bucy filter was designed for its real-time estimation from the steering angles and on-board sensors measurements

285 (see Appendix B).

4.1. Simulation Results

First, numerical simulation results are reported using ROS-GAZEBO and a virtual physical engine (cf. Figure 3). These simulations are performed in the sloping environment (i.e. slope with $\pm 15°$) to study the effectiveness of our

290 QP problem compared with the LQR controller. Two kinds of global reference paths with different characteristics are both tested with these controllers: the first one is a path with two aggressive maneuvers right and left ("Z path") plotted in Figure 5(a), and the second one is a path with a narrow right turn and small radius curvature to excite the vehicle dynamics ("O path") as shown

295 by Figure 5(b). It can be noticed that thanks to the QP problem and LQR controller, the vehicle successfully follows the desired paths at $V_x = 10m.s^{-1}$.

The simulation part is performed at high longitudinal speeds $V_x = 5m.s^{-1}$ and $V_x = 10m.s^{-1}$. The parameters of this proposed constrained path tracking controller are tuned as: the sample time $T_d = 20ms$ and the prediction

300 horizon is fixed according to the vehicle's velocity ($N_p = 20$ at $V_x = 5m.s^{-1}$ and $N_p = 40$ at $V_x = 10m.s^{-1}$). The extremum front and rear steering angles are adjusted to $\delta^{\max}_{(f,r)} = -\delta^{\min}_{(f,r)} = \pm 10°$, and their rate of change extremum is $\Delta\delta^{\max}_{(f,r)} = -\Delta\delta^{\min}_{(f,r)} = \pm 3°.s^{-1}$. The state-weighting matrix $Q_n = \text{diag}(Q, Q, \ldots, Q) \in \mathbb{R}^{q \times q}$ with $Q = \text{diag}(50, 20, 20)$, and the input-weighting

305 matrix $R_n = \text{diag}(R, R, \ldots, R) \in \mathbb{R}^{r \times r}$ with $R = \text{diag}(10^2, 10^2)$.

The friction coefficient, by the way, is assumed to be a constant value and to be the same at all wheels (i.e. $\mu_i = \mu \ \forall i \in [\![1, 4]\!]$) and invariable over a finite time horizon. Since the robot moves in grass terrain, the friction coefficient value can be approximated to $\mu = 0.35$ characterizing the rubber and grass contact

310 friction (see [35] and [36] for an overview on friction estimation techniques). Therefore, the extremum front and rear side-slip angles $\beta^{\max}_{(f,r)} = -\beta^{\min}_{(f,r)}$ can

20

be naturally computed using the inequality (17). However, it also requires the knowledge about the cornering stiffness parameters $C_{(f,r)}$ that will be estimated via the nonlinear observer described in Appendix A. The estimated parameters

315 via this observer at $V_x = 10m.s^{-1}$ are plotted in Figure 6(e) for "*Z path*" and Figure 7(e) for "*O path*". As can be seen, this observer converges very quickly when the vehicle is moving along curves with the high curvature that excites its lateral dynamics. The convergence value of the front and rear cornering stiffness is $(C_{(f,r)} \approx 16kN.rad^{-1})$ reflecting the tire-ground contact conditions of

320 GAZEBO environment. Take into account the estimated tire cornering stiffness, the side-slip angle limits can then be approximated to $\beta_{(f,r)}^{\max} = -\beta_{(f,r)}^{\min} \approx 6°$. On the other hand, the road bank and road grade angles are on-line identified using the Luenberger observer proposed in [32] (see Appendix A) in order to adapt and update the identified parameters into the controllers when new data becomes available (Figures 7(e) and 6(e)) .
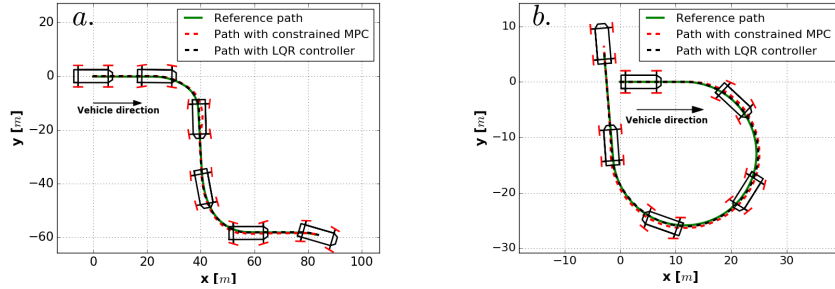

Figure 5: Reference paths and recorded ones using the constrained MPC and LQR controller at $V_x = 10m.s^{-1}$. (a) "*Z path*". (b) "*O path*".

325

To emphasize more precisely the efficiency of the proposed constrained MPC compared with the LQR controller, the front and rear steering angles at longitudinal speeds $V_x = 5m.s^{-1}$ and $V_x = 10m.s^{-1}$ are plotted in Figures 6(a)&(b) and Figures 7(a)&(b) for "*Z*" and "*O paths*", respectively. The steering angles

330 obtained with the LQR controller are depicted using the black line, and those with the MPC are in blue and red lines. We can remark that the constrained MPC and LQR controllers allow to keep them at each sampling instant between the fixed bounds ($\pm 10°$). Nevertheless, the LQR controller does not guarantee

21

their respect all the time if the conditions change (e.g. reference path, vehicle's
velocity), as can be seen by the experimental results depicted in Figure 8(d),
where the steering angles computed by the LQR controller exceed slightly the
mechanical limits. That makes the proposed constrained MPC much more in-
teresting than the LQR controller to ensure the rover's safety. Moreover, the
measured steering angles vary smoothly with small values and opposite signs to
increase the vehicle's maneuverability, that characterizes one of the most signif-
icant benefit of a double-steering systems. Nonetheless, we can note that the
property of opposite signs is no longer preserved at high speeds. This is proba-
bly due to the important sliding phenomenon and the existence of one side-slip
angle at the vehicle's center of mass that can affect significantly the symmetry
between the front and the rear side-slip angles.

It is recalled that side-slip angles can be computed using the equation (9a)
and are depicted on Figures 6(c)&(d) and Figures 7(c)&(d) for "Z" and "O
paths$", respectively, at different velocities. Once the curves are reached, these
angles become large due to high centrifugal forces along cornering and important
lateral acceleration a_y. This latter is indeed related to the square of the vehicle
longitudinal velocity and the curve curvature ($a_y = \rho V_x^2$). As mentioned before,
the LQR controller does not apply any constraints, it is for that reason that the
slip angles computed through this controller (black lines) exceed the bounds
($\pm 6°$). In contrast, those supplied by the constrained MPC are always main-
tained between them, which is a huge advantage of this controller for ensuring
robot stability and controllability (i.e. by maintaining the tire pseudo-sliding
zone).

The path tracking accuracy is an another issue that has to be studied by
using the MPC and LQR controllers. Figures 6(g)&(h) and Figures 7(g)&(h)
show the lateral and angular deviations at $V_x = 10m.s^{-1}$. As can be clearly
seen from these figures, the path tracking accuracy using the LQR controller is
better than the one given by the QP problem (e.g. for "Z paths", $e_y = 0.2m$ and
$e_\psi = 2°$ with the LQR controller at curvilinear abscissa $40m$, against $e_y = 0.5m$
and $e_\psi = -4°$ with the MPC controller). This quality of path tracking is reduced

22

³⁶⁵ because of sliding and steering constraints included in the configuration of the QP problem that must be respected during the robot task, and they cannot be handled by the LQR controller.
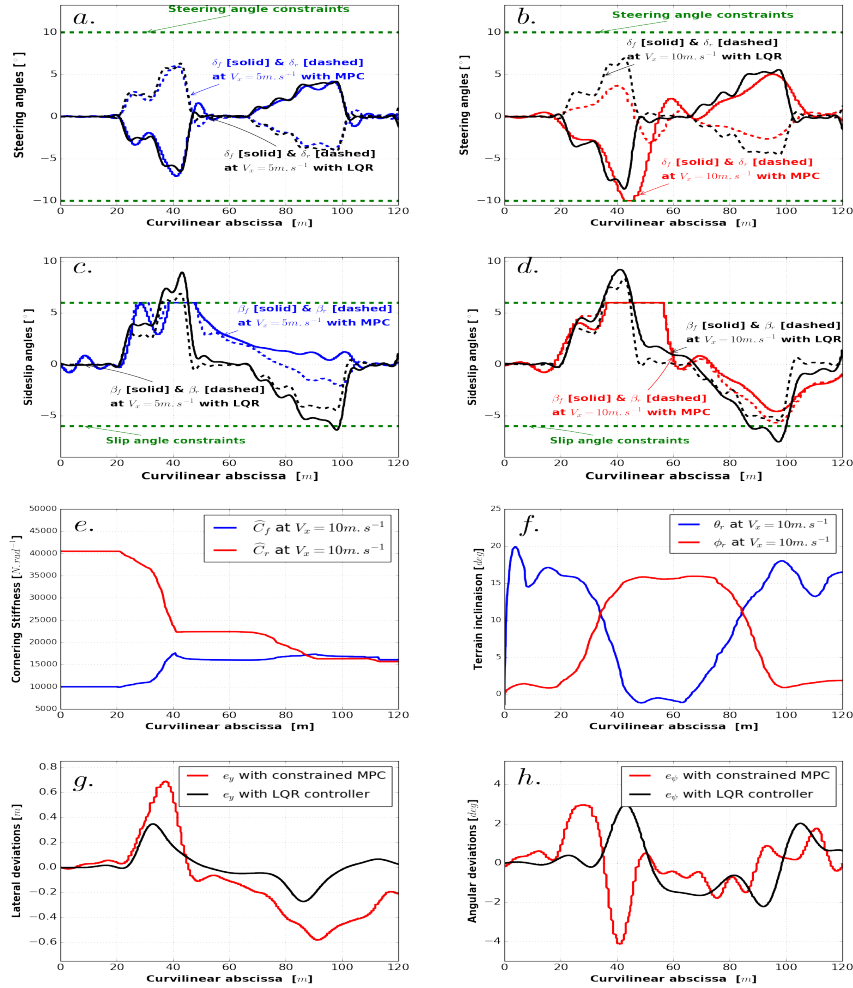

Figure 6: Simulation results of "Z path" at the velocities $V_x = 5m.s^{-1}$ and $V_x = 10m.s^{-1}$ with the constrained MPC and LQR controllers. (a) & (b) Recorded front and rear steering angles. (c) & (d) Front and rear side-slip angles. (e) Estimated front and rear tire cornering stiffness. (f) Estimated bank and grade angles. (g) & (h) Lateral and angular path tracking errors at $V_x = 10m.s^{-1}$.

To summarize, the simulation results provided by the MPC controller are more relevant than the ones obtained by the LQR controller. Both of them allow ³⁷⁰ the robot to successfully track different desired path with small and smooth

23

inputs. However, the LQR controller does not guarantee any steering and sliding constraints that are critical and necessary for the vehicle stability and safety, and where all of them are fulfilled by the constrained MPC. To show clearly the limits of the LQR controller, we plan in our future works to perform other experiments and tests when the vehicle roll (roll angle control) and longitudinal (V_x control) dynamics will be integrated.
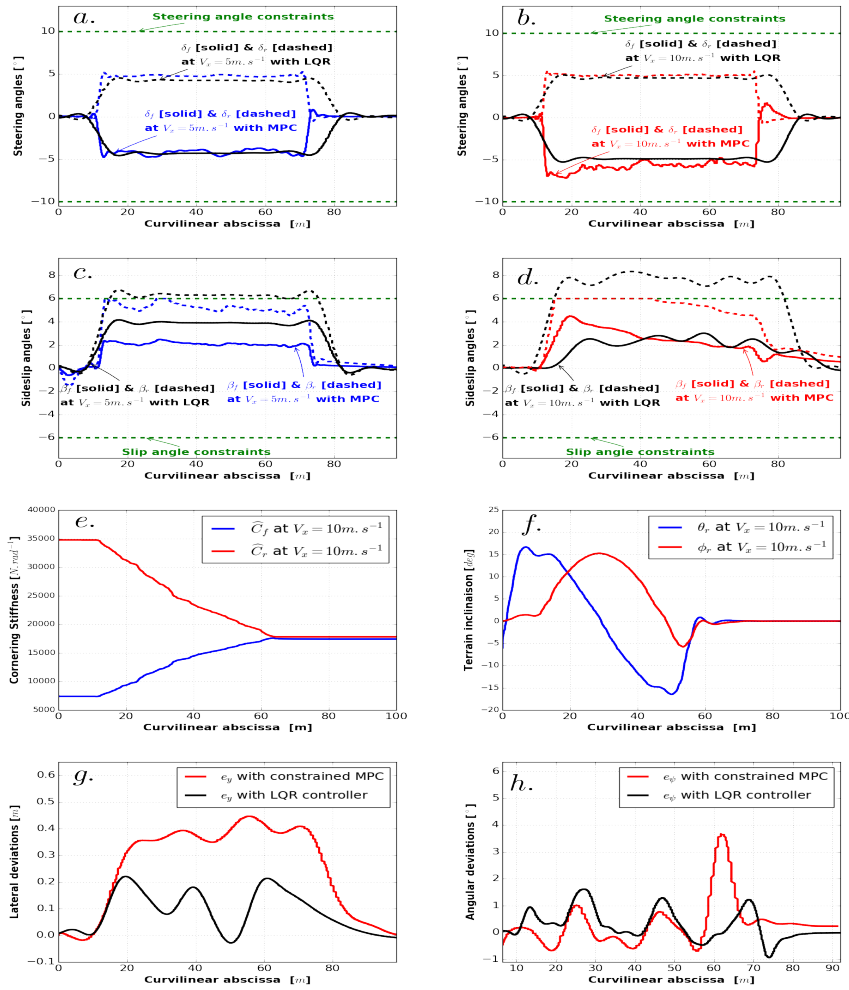

Figure 7: Simulation results of "O $path$" at the velocities $V_x = 5m.s^{-1}$ and $V_x = 10m.s^{-1}$ with the constrained MPC and LQR controllers. (a) & (b) Recorded front and rear steering angles. (c) & (d) Front and rear side-slip angles. (e) Estimated front and rear tire cornering stiffness. (f) Estimated bank and grade angles. (g) & (h) Lateral and angular path tracking errors at $V_x = 10m.s^{-1}$.

24

4.2. Experimental Results

The constrained MPC and LQR controllers are implemented on a test double-steering vehicle shown in Figure 4. These controllers are validated with the same settings as the simulation part. The experiments are performed on a flat ground (assuming $\theta_r = \phi_r = 0°$) at the longitudinal velocities $V_x = 2.5 m.s^{-1}$ and $V_x = 4 m.s^{-1}$. The experimental results are summarized in Figure 8. In all tests, the extremum steering angles are $\pm 10°$ and their rate of change limit is $\pm 3°.s^{-1}$, the slip-angle extremum is $\pm 6°$, the road friction coefficient is approximately 0.35 and the prediction horizon $N_p = 10$. The controllers were run in a powerful Intel Nuc (with a core $i7 - 7567U$, $3, 5 GHz$) feeding the low-level control with the required optimal front and rear steering angles needed to perform the tracking task. Onboard sensors and tested controllers are invoked every $100ms$. In order to effectively remove certain frequencies of noise related to the experimental issues, all signals, before they can be used, are filtered by applying an eight-order low-pass butterworth filter with small cut-off frequency.

To demonstrate the usefulness of our approach, we compare it with the previously proposed controller in [27] under the same conditions. Figure 8(a) shows the desired path and recorded ones at $V_x = 4 m.s^{-1}$ supplied by the constrained MPC (red line) and LQR controller (black line). We choose a reference path with a small radius curvature so as to obtain high lateral acceleration that can excite the vehicle lateral motion. As can be seen, the car tracks efficiently the desired path thanks to these controllers. However, the LQR controller appears more accurate than the constrained MPC because it does not consider any steering or sliding constraints. This can be noted from Figures 8(g) and 8(h) showing the lateral and angular errors (e.g., $e_y = 0.5m$ and $e_\psi = 2.5°$ with LQR controller at curvilinear abscissa $40m$, whereas with MPC controller $e_y = 0.9m$ and $e_\psi = 5.5°$).

For the results presented below, the estimation algorithm presented in [6] is implemented to estimate the front and rear tire cornering stiffness $C_{(f,r)}$ (Appendix A), which are thereafter used to feed the controllers with adequate parameters as new data becomes available (see Figure 8(b)). They converge to

25

the same value in steady state ($C_{(f,r)} \approx 28kN.rad^{-1}$). This value is important due to the fact that the robot is moving on a quite good grip ground conditions (dry-grass ground). We also note that between the curvilinear abscissa 0 and $10m$, the estimated parameters remain almost constant because the trajectory is a straight line that does not excite the vehicle dynamics. Besides from the start of the turn between 10 and $15m$, they converge quickly but remains constant between $15m$ and $20m$, which is probably the steady state of the circular part of the reference path.

Figures 8(c) and 8(d) show the computed steering angles $\delta_{(f,r)}$ needed to keep the vehicle close to the desired path at the longitudinal speeds $V_x = 2.5m.s^{-1}$ and $V_x = 4m.s^{-1}$ (black line for LQR controller, red and blue lines for the constrained MPC). We note that, the magnitude of $\delta_{(f,r)}$ is too small and smooth, and is always maintained between fixed bounds $\pm 10°$ thanks to the QP problem. Compared to the constrained MPC, the steering angles given by the LQR controller exceed the limits imposed by the mechanical stops of the vehicle at $V_x = 4m.s^{-1}$ (see Figure 8(d)), which is undesirable for the system safety particularly when the robot tracks complex reference paths (i.e. with big curvature) at high speeds. Consequently, the MPC corrects the robot's control action to avoid the constraint violation.

Furthermore, Figures 8(e) and 8(f) plot the front and rear sliding angles $\beta_{(f,r)}$ for both studied scenarios, MPC and LQR controllers, at $V_x = 2.5m.s^{-1}$ and $V_x = 4m.s^{-1}$. At low speeds, these angles seem too small due to weak centrifugal forces and small lateral acceleration ($a_y = \rho V_x^2$). Although, when the vehicle velocity increases, they become much more significant as can be noticed from Figure 8(f). For the LQR controller, the considered limits are violated at $V_x = 4m.s^{-1}$, even though the constrained MPC guarantees the pseudo-sliding area bounds at each time-step, i.e. they lie within $\pm 6°$.

As a conclusion, the constrained MPC seems much more interesting than the LQR controller for ensuring the path tracking task and fulfilling the steering and sliding constraints. As mentioned before, these constraints affect slightly the path tracking accuracy. This point will be treated in our future works to

26

enhance the efficiency of the MPC controller. In fact, the performance of the

440 considered strategy could potentially be much more promising by incorporating other control inputs (e.g., vehicle longitudinal speed V_x control) and other constraints to increase more the vehicle stability and safety (such as limiting the lateral acceleration a_y and roll angle ϕ).
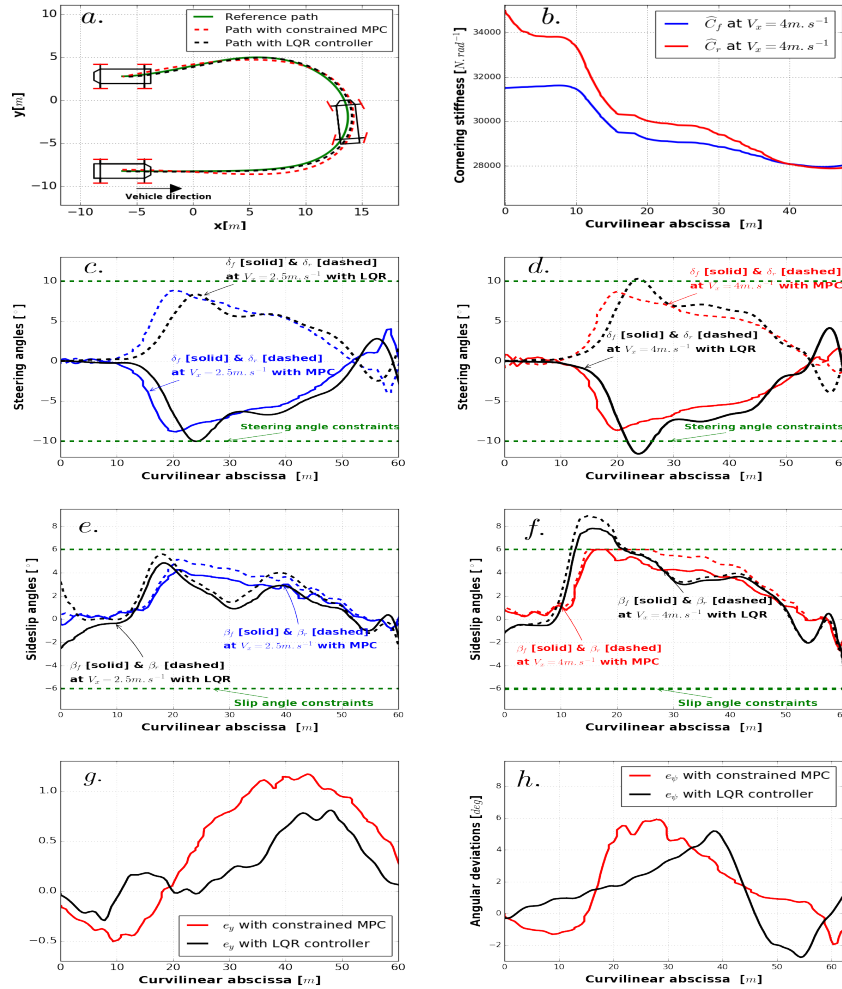

Figure 8: Experimental results with the constrained MPC and LQR controller at the velocities $V_x = 2.5 m.s^{-1}$ and $V_x = 4 m.s^{-1}$. (a) Reference path and recorded ones. (b) Estimated cornering stiffness. (c) & (d) Recorded front and rear steering angles. (e) & (f) Front and rear side-slip angles. (g) & (h) Lateral and angular path tracking deviations at $V_x = 4 m.s^{-1}$.

27

5. Conclusions & Future Work

⁴⁴⁵ Off-road robots are intended to traverse different kinds of terrains with different conditions of friction and cohesion. In such dynamic and non-predictable environment, several criteria must be satisfied with the safety and stability as the most important ones. In the work presented in this paper, a constrained model predictive control (MPC) is synthesized and applied for the dynamic path tracking dedicated to off-road mobile robots with a double-steering axle (it can also be easily extended to single-steering rovers). The main advantage of the MPC is indeed the ability to anticipate future changes in set-points and handle constraints that are critical and necessary for the safety and stability of the vehicle. This controller is based on a dynamic model that includes the wheel-ground lateral slippage and terrain geometry parameters. It is formulated as an optimization problem that computes at each time-step the optimal and dynamically-consistent front and rear steering angles required to perform a desired path, with respect to multiple constraints, essentially the steering joint limits and the tire adhesion area bounds (i.e., pseudo-sliding zone limits). To demonstrate the capability of the proposed controller, it is compared with another previously designed control law, which is based on the LQR strategy and the same dynamic model. However, it does not take into account any physical constraints of the system, which is not a beneficial point to emphasize their importance to make the vehicle safe and stable. Finally, we show simulation results under ROS/GAZEBO detailing the behavior of the proposed controller compared with the LQR one, as well as experimental results obtained by implementing the proposed framework controller in a real off-road mobile robot. The results prove the capability of the constrained MPC to manage effectively the path tracking task while respecting at each sampling time the steering and sliding constraints, that are not applied by the LQR controller. Moreover, the proposed constrained MPC seems to be less accurate than the LQR controller due to the critical constraints fulfilled by the constrained MPC at each time-step, which affect its performances once they are reached.

Besides, the longitudinal dynamics (control of V_x) were not considered in this study. We anticipate to integrate the control of the longitudinal dynamics into our QP problem in order to improve its performance particularly the tracking accuracy. Indeed, such a control will enable the vehicle to mitigate its forward speed mainly along turns where the curvature is maximum (transient regime). Moreover, this longitudinal speed must always fill an inequality which depends on the curvature of the desired path ρ and the friction coefficient μ : $V_x \leq \sqrt{\frac{\mu g}{\rho}}$. On the other hand, it would also be interesting to incorporate other constraints related to the vehicle stability. We particularly plan to constrain the lateral acceleration and the robot roll angle to prevent the robot from generating harmful lateral motions (such as the vehicle rollover or spin around during cornering). These new constraints require new formulations taking into account the prediction horizon and optimization variable.

Appendix A : Environmental Parameters Estimation

In this appendix, our motivation is to ensure high accuracy and stability of the proposed QP problem developed in section 3. This controller is based on the dynamic model by taking into account the wheel/ground contact conditions ($C_{(f,r)}$) and the environment geometry variables (θ_r and ϕ_r). Hence, the real-time adaptation of these parameters is crucial to get good outcomes of the path tracking task. This estimation is not the purpose of this paper. Nevertheless, we remind some observers that have already been developed in our previous works to estimated accurately these parameters [32] and [6].

Cornering Stiffnesses Estimation

The nonlinear observer based was designed in [6] for on-line estimation of the front and rear tire cornering stiffness ($C_{(f,r)}$). This observer makes use of the lateral velocity V_y, the yaw rate V_ψ and the steering angles $\delta_{(f,r)}$. We

summarize here the equation of this nonlinear observer,

$$\begin{cases} \dot{\Lambda} = -G(x,u)\Lambda - G(x,u)\left[B_c^{-1}A_c x + \Upsilon - c(x,u)\right] \\ \widehat{\omega}_c = \Lambda + c(x,u) \end{cases} \tag{26}$$

where the variables $\Lambda, x, u, A_c, B_c, G, c, \widehat{\omega}_c$ and Υ can be reviewed in more details in [6].

Terrain Geometry Estimation

Since the environment geometry is intended to be changed mainly in the off-road context, the estimation of the bank and grade angles (θ_r and ϕ_r) is necessary (particularly when the vehicle moves across a slope) to compensate the gravity components in the dynamic model. For this issue, one linear Luenberger observer was previously stated in [32] to estimate on-line terrain geometry angles. This observer is based on the yaw rate, lateral velocity and IMU measurements. Finlay, the estimated parameters are then fed in our new controller to enhance its efficiency. The standard observer equation can be reminded as:

$$\widehat{x}_{r[k+1]} = A_r\widehat{x}_{r[k]} + B_r u_{r[k]} + L\tilde{x}_{r[k]} \tag{27}$$

where $\widehat{x}_{r[k]}$ and $u_{r[k]}$ are the observer state and control variable respectively. $\tilde{x}_{r[k]}$ is the observer error. A_r and B_r are observer state matrices. L is the Luenberger observer gain matrix (see [32] for more details).

Appendix B : state observer - Kalman-Bucy Filter

Embedded sensors allow to measure V_ψ, e_y and e_ψ. In order to estimate the lateral speed V_y and complete the state vector needed for computing the control input, a linear Kalman-Bucy observer was designed in this appendix. This observer assumes the knowledge of the robot dynamic model and then the ground geometry and wheel-ground contact parameters. Its inputs are y, u, A, B, C, Γ_ς, Γ_γ (the error covariance matrices) and dt (the sampling time of

discretization). Its on-line calculated variables are the Kalman Bucy gain K_b, the estimated state $\widehat{\xi}$ and the state covariance matrix Γ_t (see equation (28)).

$$
\begin{cases}
\dot{\widehat{\xi}} = A(\widehat{\xi} - \xi_{ss}) + K_b(y - C(\widehat{\xi} - \xi_{ss})) + B(u - u_{ss}) \\
\dot{\Gamma}_t = A\Gamma_t + \Gamma_t A^T - K_b\Gamma_\gamma K_b^T + \dfrac{1}{dt^2}\Gamma_\varsigma \\
K_b = \Gamma_t C^T \Gamma_\gamma^{-1}
\end{cases}
\tag{28}
$$

Appendix C : LQR controller

From the dynamic model given in (2), the feedback control law that minimizes the LQR cost function can be derived as follows (see [27]),

$$
u = Ny_d - K(\widehat{\xi} - \xi_{ss}) + u_{ss}
\tag{29}
$$

with y_d is the desired set-point, $\widehat{\xi} = [\widehat{V}_y, \widehat{V}_\psi, \widehat{e}_y, \widehat{e}_\psi]^T$ is the observed state by Kalman-Bucy filter and the gain matrices N, K are expressed in (30).

$$
K = R^{-1}B^T P_r \qquad \text{and} \qquad N = [C[A - BK]^{-1}B]^{-1}
\tag{30}
$$

where P_r is the algebraic solution of the Riccati equation depending on Q and R which are the state-weighting and the input-weighting matrices respectively.

Acknowledgments

References

R. DeSantis, Path-tracking for car-like robots with single and double steering, IEEE Transactions on vehicular technology 44 (2) (1995) 366–377.

C. Cariou, R. Lenain, B. Thuilot, P. Martinet, Adaptive control of four-wheel-steering off-road mobile robots: Application to path tracking and heading control in presence of sliding, in: 2008 IEEE/RSJ International Conference on Intelligent Robots and Systems, IEEE, 2008, pp. 1759–1764.

A. De Luca, G. Oriolo, C. Samson, Feedback control of a nonholonomic car-like robot, in: Robot motion planning and control, Springer, 1998, pp. 171–253.

B. D'Andrea-Novel, G. Campion, G. Bastin, Control of wheeled mobile robots not satisfying ideal velocity constraints: a singular perturbation approach, International Journal of Robust and Nonlinear Control 5 (4) (1995) 243–267.

R. Lenain, B. Thuilot, C. Cariou, P. Martinet, Mixed kinematic and dynamic sideslip angle observer for accurate control of fast off-road mobile robots, Journal of Field Robotics 27 (2) (2010) 181–196.

M. Fnadi, F. Plumet, F. Benamar, Nonlinear tire cornering stiffness observer for a double steering off-road mobile robot, in: 2019 International Conference on Robotics and Automation (ICRA), IEEE, 2019, pp. 7529–7534.

N. H. Amer, H. Zamzuri, K. Hudha, Z. A. Kadir, Modelling and control strategies in path tracking control for autonomous ground vehicles: a review of state of the art and challenges, Journal of intelligent & robotic systems 86 (2) (2017) 225–254.

C. Katrakazas, M. Quddus, W.-H. Chen, L. Deka, Real-time motion planning methods for autonomous on-road driving: State-of-the-art and future research directions, Transportation Research Part C: Emerging Technologies 60 (2015) 416–442.

K. Goris, Autonomous mobile robot mechanical design, VrijeUniversiteitBrussel, Engineering Degree Thesis, Brussels, Belgium.

M. Krid, F. Benamar, Z. Zamzami, Design of an active device for controlling lateral stability of fast mobile robot, Robotica 34 (11) (2016) 2629–2651.

32

₅₆₅ N. Bouton, R. Lenain, B. Thuilot, J.-C. Fauroux, A rollover indicator based on the prediction of the load transfer in presence of sliding: application to an all terrain vehicle, in: Proceedings 2007 IEEE International Conference on Robotics and Automation, IEEE, 2007, pp. 1158–1163.

D. Leith, W. Leithead, M. Vilaplana, Robust lateral controller for 4-wheel steer

₅₇₀ cars with actuator constraints, in: Proceedings of the 44th IEEE Conference on Decision and Control, IEEE, 2005, pp. 5101–5106.

M. Spenko, Y. Kuroda, S. Dubowsky, K. Iagnemma, Hazard avoidance for high-speed mobile robots in rough terrain, Journal of Field Robotics 23 (5) (2006) 311–331.

₅₇₅ S.-T. Peng, J.-J. Sheu, C.-C. Chang, A control scheme for automatic path tracking of vehicles subject to wheel slip constraint, in: Proceedings of the 2004 American Control Conference, Vol. 1, IEEE, 2004, pp. 804–809.

T. Bächle, K. Graichen, M. Buchholz, K. Dietmayer, Slip-constrained model predictive control allocation for an all-wheel driven electric vehicle, IFAC

₅₈₀ Proceedings Volumes 47 (3) (2014) 12042–12047.

W. Du, M. Fnadi, F. Benamar, Rolling based locomotion on rough terrain for a wheeled quadruped using centroidal dynamics, Mechanism and Machine Theory 153 (2020) 103984.

P. Falcone, M. Tufo, F. Borrelli, J. Asgari, H. E. Tseng, A linear time varying

₅₈₅ model predictive control approach to the integrated vehicle dynamics control problem in autonomous systems, in: 2007 46th IEEE Conference on Decision and Control, IEEE, 2007, pp. 2980–2985.

P. T. Boggs, J. W. Tolle, Sequential quadratic programming, Acta numerica 4 (1995) 1–51.

₅₉₀ J. A. D. Sandretto, A. Chapoutot, Dynbex: a differential constraint library for studying dynamical systems, 2016.

33

F. Borrelli, P. Falcone, T. Keviczky, J. Asgari, D. Hrovat, Mpc-based approach to active steering for autonomous vehicle systems, International Journal of Vehicle Autonomous Systems 3 (2) (2005) 265–291.

595 A. Gray, Y. Gao, T. Lin, J. K. Hedrick, H. E. Tseng, F. Borrelli, Predictive control for agile semi-autonomous ground vehicles using motion primitives, in: 2012 American Control Conference (ACC), IEEE, 2012, pp. 4239–4244.

Y. Gao, A. Gray, J. V. Frasch, T. Lin, E. Tseng, J. K. Hedrick, F. Borrelli, Spatial predictive control for agile semi-autonomous ground vehicles, in: 600 Proceedings of the 11th international symposium on advanced vehicle control, no. 2, 2012, pp. 1–6.

J. A. dit Sandretto, Reliable nonlinear model-predictive control via validated simulation, in: 2018 Annual American Control Conference (ACC), IEEE, 2018, pp. 609–614.

605 C. J. Ostafew, A. P. Schoellig, T. D. Barfoot, Robust constrained learning-based nmpc enabling reliable mobile robot path tracking, The International Journal of Robotics Research 35 (13) (2016) 1547–1563.

P. Falcone, F. Borrelli, J. Asgari, H. E. Tseng, D. Hrovat, Predictive active steering control for autonomous vehicle systems, IEEE Transactions on 610 control systems technology 15 (3) (2007) 566–580.

T. Keviczky, P. Falcone, F. Borrelli, J. Asgari, D. Hrovat, Predictive control approach to autonomous vehicle steering, in: 2006 American Control Conference, IEEE, 2006, pp. 6–pp.

M. Fnadi, B. Menkouz, F. Plumet, F. B. Amar, Path tracking control for a 615 double steering off-road mobile robot, in: ROMANSY 22–Robot Design, Dynamics and Control, Springer, 2019, pp. 441–449.

H. B. Pacejka, Tyre and vehicle dynamics, ed, SAE International 2.

H. Dugoff, P. S. Fancher, L. Segel, Tire performance characteristics affecting vehicle response to steering and braking control inputs, Tech. rep. (1969).

620   M. Blundell, D. Harty, Multibody systems approach to vehicle dynamics, Elsevier, 2004.

Y. Wang, S. Boyd, Fast model predictive control using online optimization, IEEE Transactions on control systems technology 18 (2) (2009) 267–278.

M. Fnadi, F. Plumet, F. B. Amar, Road bank and road grade angles estimation

625   for a double steering off-road mobile robot, in: IFToMM World Congress on Mechanism and Machine Science, Springer, 2019, pp. 1771–1780.

M. S. Andersen, J. Dahl, L. Vandenberghe, Cvxopt: A python package for convex optimization, version 1.1. 6, Available at cvxopt. org 54.

M. Fnadi, D. Wenqian, G. Rafael, F. Plumet, F. Benamar, Local obstacle-

630   skirting path planning for a fast bi-steerable rover using bziers curves, in: 2020 International Conference on Robotics and Automation (ICRA), IEEE, 2020, pp. 1–8.

C.-S. Liu, H. Peng, Road friction coefficient estimation for vehicle path prediction, Vehicle system dynamics 25 (S1) (1996) 413–425.

635   R. Wang, J. Wang, Tire–road friction coefficient and tire cornering stiffness estimation based on longitudinal tire force difference generation, Control Engineering Practice 21 (1) (2013) 65–75.